Albedo effect on radiative errors in air temperature measurements

Hendrik Huwald,[1] Chad W. Higgins,[1] Marc-Olivier Boldi,[1] Elie Bou-Zeid,[2] Michael Lehning,[3] and Marc B. Parlange[1]

Received 14 November 2008; revised 27 May 2009; accepted 10 June 2009; published 25 August 2009.

[1] Most standard air temperature measurements are subject to significant errors mainly due to sensor heating by solar radiation, even when the measurement principle is accurate and precise. We present various air temperature measurements together with other measurements of meteorological parameters using different sensor systems at a snow-covered and a vegetated site. Measurements from naturally ventilated air temperature sensors in multiplate shields are compared to temperatures measured using sonic anemometers which are unaffected by solar radiation. Over snow, 30 min mean temperature differences can be as large as 10°C. Unshielded thermocouples were also tested and are generally less affected by shortwave radiation. Temperature errors decrease with decreasing solar radiation and increasing wind speed but do not completely disappear at a given solar radiation even in the presence of effective ventilation. We show that temperature errors grow faster for reflected than for incident solar radiation, demonstrating the influence of the surface properties on radiative errors, and we detect the albedo as a variable with major influence on the magnitude of the error as well as a key quantity in possible error correction schemes. An extension is proposed for an existing similarity regression model to correct for radiative errors; thus, surface-reflected shortwave radiation is identified as a principal source of error and the key variable for obtaining a unique nondimensional scaling of radiative errors.

Citation: Huwald, H., C. W. Higgins, M.-O. Boldi, E. Bou-Zeid, M. Lehning, and M. B. Parlange (2009), Albedo effect on radiative errors in air temperature measurements, *Water Resour. Res.*, *45*, W08431, doi:10.1029/2008WR007600.

1. Introduction

[2] Air temperature is one of the most frequently measured meteorological variables and is used for numerous purposes such as time series analyses, model forcing or validation, and computation of dependent key quantities such as sensible heat flux or snow and ice melt in temperature-index models [e.g., *Brutsaert and Parlange*, 1992; *Katul and Parlange*, 1995; *Hock*, 1999; *Braithwaite and Zhang*, 2000; *Ohmura*, 2001]. However, accurate air temperature measurements are difficult to obtain, in particular over snow-covered terrain with high albedo, since most sensors used to measure air temperature are subject to errors due to radiative heating in the presence of solar radiation and low wind speed [*Arck and Scherer*, 2001; *Georges and Kaser*, 2002; *Lundquist and Huggett*, 2008]. The problem of temperature errors due to radiation (hereafter referred to as radiative errors) is well known and has been discussed in numerous studies at many different locations [e.g., *Fuchs and Tanner*, 1965; *Anderson and Baumgartner*, 1998; *Richardson et al.*, 1999; *Erell et al.*, 2005; *Nakamura and Mahrt*, 2005]. These errors can easily be on the order of several degrees [*Arck and Scherer*, 2001; *Hardy et al.*, 1998; *Lundquist and Huggett*, 2008]. In addition, they depend not only on the magnitude of the radiative heat flux and the wind speed, but also on the zenith angle of the sun [*Georges and Kaser*, 2002; *Nakamura and Mahrt*, 2005]. Air temperature measurements are not always corrected for radiative errors, or applied correction schemes are not able to entirely eliminate these errors from the observations; this may have substantial implications and consequences for all conclusions relying on air temperature measurements.

[3] To minimize measurement errors resulting from solar heating, sensors are typically mounted in special housings intended to protect the sensor from solar radiation while still allowing for easy and sufficient exchange of air with the ambient atmosphere. The most common design among a variety of housings is a stacked multiplate shield broadly used on thousands of meteorological stations, in particular on automated weather stations at remote locations were power supply is an issue. The specific geometry and design of different shields, mostly optimized to reduce the effect of direct incident solar radiation, determine their effectiveness in terms of radiation protection and possible airflow [*Hubbard et al.*, 2001; *Lin et al.*, 2001]. However, such naturally ventilated housings can only reduce the effect of radiative heating and the resulting bias in the temperature measurements, but not completely eliminate errors. Incident and reflected shortwave radiation is partially absorbed by the housing which then transfers sensible heat and infrared radiation to the actual sensor depending on the geometry, mass and thermal properties of both the shield and the

[1] School of Architecture, Civil and Environmental Engineering, Ecole Polytechnique Fédérale de Lausanne, Lausanne, Switzerland.
[2] Department of Civil and Environmental Engineering, Princeton University, Princeton, New Jersey, USA.
[3] WSL Institute for Snow and Avalanche Research SLF, Davos, Switzerland.

0043-1397/09/2008WR007600$09.00

sensor. Also, conductive heat transfer can act as a source of error for certain sensor types or instruments (e.g., thermocouples, thermistors) when parts of the sensor are exposed to solar radiation. According to *Richardson et al.* [1999], an optimal shield (1) minimizes the radiation reaching the sensor, (2) minimizes the radiation absorbed by the shield, and (3) maximizes airflow around the sensor. In addition, it protects from riming, dirt deposition and other environmental impacts.

[4] If sufficient power is available, mechanically ventilated radiation shields are used instead of naturally ventilated sensor housings. In contrast to naturally ventilated radiation shields, the aspiration efficiency in mechanically ventilated shields does not depend on the wind speed and the specific shield geometry. Mechanically ventilated sensors are often used as reference instruments for naturally ventilated sensors. To date, many studies have been carried out to intercompare different types of radiation shields and to quantify radiative errors [e.g., *Gil*, 1983; *Payne*, 1987; *Hock*, 1994; *Erell et al.*, 2005]. All these studies conclude that in the presence of solar radiation and low wind speed conditions the shield absorbs energy which heats the air and the sensor internally. Natural ventilation is often not sufficient to effectively ventilate the shield [*Georges and Kaser*, 2002], with the consequence that the shield temperature can exceed the air temperature by several degrees [*Nakamura and Mahrt*, 2005]. Radiative errors described in many shield intercomparison studies differ considerably depending on the type of temperature sensor, radiation shield, reference sensor, the surface properties of the ground, the location, and actual weather conditions, for instance up to 2°C over grassland [*Nakamura and Mahrt*, 2005] and up to 10°C over snow [*Hardy et al.*, 1998]. A few studies identify surface-reflected solar radiation as having a major impact on the radiative error [*Arck and Scherer*, 2001; *Georges and Kaser*, 2002]. Also, a substantial fraction of (surface-reflected) solar radiation entering a multiplate radiation shield from below is absorbed in the shield interior [*Richardson et al.*, 1999; *Arck and Scherer*, 2001] which leads to an increase in magnitude of the radiation error. The wide range of degree day factors from several studies might not only be a result of geomorphologic and climatologic site characteristics, but may simply be a direct consequence of biased air temperature measurements taken over various surfaces with different reflective properties [*Braithwaite and Zhang*, 2000].

[5] Several methods have been proposed to correct for radiative errors [*Kent et al.*, 1993; *Anderson and Baumgartner*, 1998; *Hock*, 1999; *Arck and Scherer*, 2001; *Georges and Kaser*, 2002; *Nakamura and Mahrt*, 2005; *Mauder et al.*, 2008]. For instance, *Arck and Scherer* [2001] developed a physically based method using wind speed and upwelling shortwave radiation for the computation of corrections. *Georges and Kaser* [2002] modeled the error and used this information to account for the bias in the observations, while *Nakamura and Mahrt* [2005] used a similarity regression model, scaling the incident shortwave radiation with the internal energy of the air using the wind speed and the uncorrected measured air temperature.

[6] The present study investigates radiative errors observed during three multiweek field campaigns in 2007 and 2008 at two very different locations with particular focus on the influence of surface properties on the radiative error. We show some extreme cases of biased temperature measurements and identify the responsible physical processes and conditions. Unlike many previous studies, a sonic anemometer is used as a reference sensor for the air temperature measurements. While sonic anemometers are not usually considered as instruments to reliably measure the mean temperature, they are undoubtedly unaffected by radiation and are therefore suitable to study the influence of radiation on air temperature measurements. In addition, as will be explained below, attention was given to ensure good accuracy of the sonic measurements. The study examines the role of the albedo in the context of radiative errors. We also develop an extension of the *Nakamura and Mahrt* [2005] scaling model accounting for the findings of this work, particularly the importance of the surface albedo.

[7] The next section presents the experimental setup of the field sites followed by section 3 which deals with air temperature measurement theory. The analysis of the observations and the results are discussed in section 4 and summarized in section 5.

2. Experimental Setup

2.1. Plaine Morte Glacier (GPM07 and GPM08)

[8] To investigate snow-atmosphere interactions, radiative and turbulent heat fluxes and other meteorological parameters were measured at the Plaine Morte glacier, near Crans-Montana in the Swiss Alps during the winters of 2006–2008. The data presented here were acquired during the winter seasons of 2007 (5 February through 10 April) and 2008 (8 February through 11 March), and air temperature data span a range from about −20 to 5°C with typical diurnal variations of 5 to 15°C. The Plaine Morte glacier (GPM) is a seasonally snow-covered, relatively flat glacier of about 10 km^2 (5 km east–west, 2 km north–south) with a mean altitude of roughly 2700 m above sea level (asl). The experimental site was located at the center of the eastern part of the glacier at an altitude of 2770 m asl, where a meteorological station was installed measuring incoming and reflected solar radiation, downward and outgoing longwave radiation, air temperature, relative humidity, wind speed, wind direction, snow surface temperature, barometric pressure, and snow surface elevation. The station also included several three-dimensional sonic anemometers and open path infrared water vapor and carbon dioxide gas analyzers for eddy covariance studies. Air temperature sensors (RTD Pt100 thermistor, Rotronic MP103A) were mounted in R. M. Young Instruments, model 41003, multiplate solar radiation shields.

[9] Upward and downward looking pyranometers and pyrgeometers (Kipp and Zonen CM21 and CG4) were mounted on a south facing boom with each sensor actively ventilated by means of a small fan and covered by a hemispherical housing (ventilation and heating system, PMOD-VHS, Davos, Switzerland). Eddy covariance instruments (Campbell Scientific CSAT3 and LI-COR LI-7500) were installed at the same level as the air temperature sensors and cup anemometers (Vector Instruments A100R). In 2007, eddy covariance measurements were taken at one level only (initially at 2.45m height); in 2008, sensors were installed at four levels with 1m vertical

spacing, and the lowest initially at 0.95 m above the snow surface. The 2008 setup included a thermocouple (Campbell Scientific, type E) next to each CSAT3. During the season, snow accumulation (precipitation and blowing snow) changed the instrument heights above the surface, and the sensors were manually lifted when needed. In this study, only data from sensors mounted at level three are presented since this level is comparable to the geometric setup of instruments in the other two experiments described in this section. The sonic anemometers were fixed at a horizontal distance of about 1m from the shielded thermistors. Eddy covariance instruments were oriented such that they were facing the predominant wind direction during cold and dry weather conditions, with a homogeneous flat upstream fetch of about 1.5 km. The sampling frequency was 20 Hz for the eddy covariance sensors and one minute (average of six measurements at 0.1 Hz) for all other sensors. In the following analysis, the data have been aggregated to corresponding 30 min averages.

2.2. TABLES Experiment

[10] In the context of an extensive field experiment investigating the characteristics of the surface and boundary layer over different surfaces (Turbulent Atmospheric Boundary Layer Using Lidar, Eddy Covariance, and Scintillometry (TABLES)), an energy balance station was installed on a flat clover field at a distance of about 100 m from a small lake (Seedorf, Switzerland). The station was equipped with a shielded temperature and humidity probe, cup and sonic anemometers, thermocouple, upward and downward looking pyranometers and pyrgeometers, and an open path infrared water vapor and carbon dioxide gas analyzer (all of the same sensor types as in the GPM deployments). The observational data set spans a period from 13 August through 5 September 2008, and a temperature range from about 5 to 30°C with typical diurnal variations of approximately 15°C. The thermocouple junction was mounted next to the measuring volume of the sonic anemometer. Wind speed, air temperature and relative humidity were all measured at the level of the sonic anemometer at 2.5 m above the surface and within less than 3m horizontal distance from each other. Identical to the GPM experiment, the data were sampled at a frequency of 20 Hz for the eddy covariance sensors and one minute (average of six measurements at 0.1 Hz) for the other sensors. The data have been aggregated to corresponding 30 min averages.

3. Sonic Thermometry

[11] In this study, sonic anemometers were used as reference sensors to measure air temperature. In contrast to most conventional temperature sensors, a sonic anemometer determines the air temperature (virtual temperature) of an air volume independently from the instrument's temperature, representing an ideal fast response air temperature sensor. Like the surrounding atmosphere, the measured air volume is exposed to radiative fluxes and atmospheric motion, and undisturbed by any sensor shield. The transducers of each axis of a three-dimensional sonic anemometer pulse a signal while the travel time t_f to the receiver is measured. Concurrently, a signal is pulsed in the opposite direction while the travel time t_r is measured. The travel times are equal to the known distance d between the transducer heads divided by the sum of the speed of sound in moist air, c, (which is a function of temperature and humidity) and the instantaneous wind speed u along the transducer axis,

$$t_f = \frac{d}{c+u} \text{ and } t_r = \frac{d}{c-u}. \quad (1)$$

Adding the inverse of the two expressions yields an equation which can be used to compute c (m s^{-1}) using the measured travel times and the transducer spacing:

$$c = \frac{d}{2}\left(\frac{1}{t_f} + \frac{1}{t_r}\right). \quad (2)$$

The speed of sound is a function of temperature and humidity. The sonic virtual temperature can be expressed considering the humidity effect on the speed of sound [*Fleagle and Businger*, 1980; *Kaimal and Gaynor*, 1991] as

$$c^2 = \gamma_d R_d T_s = \gamma_d R_d T(1 + 0.51q), \quad (3)$$

where γ_d is the ratio of the specific heat of dry air at constant pressure to that at constant volume expressed in terms of energy (equal to 1.4, dimensionless), R_d the specific gas constant of dry air (J kg^{-1} K^{-1}), T_s the sonic virtual temperature (K), T the air temperature (K), and q the specific humidity (kg kg^{-1}). The sonic virtual temperature is proportional to c^2, with the product of γ_d and R_d as the proportionality constant. The air temperature in Celsius can be calculated as

$$T = \frac{T_s}{(1 + 0.51q)} - 273.15. \quad (4)$$

In cold environments, the specific humidity is generally very low. For the observed range of the specific humidity at the GPM site (generally smaller than 5×10^{-3} kg kg^{-1}) conversion of the sonic virtual temperature to air temperature had little impact relative to the effect we investigate (0.7 K at maximum). At TABLES, ($q < 14 \times 10^{-3}$ kg kg^{-1}), air temperature and sonic virtual temperature could differ by up to 2.1 K. The sonic virtual temperatures were converted to air temperatures in all experiments according to equation (4).

[12] Well calibrated sonic anemometers provide a good temperature resolution and relative accuracy although they may have a bias and a drift over longer time spans. The bias in temperature measurements from sonic anemometers is mainly related to the accuracy of the path length d. Careless mishandling, bumping or shaking that slightly alters d, for example by ~1 mm which is equal to about 1%, can lead to the same relative error in c (1%) but to the double of that error in T_s (2%) since it is related to the square of c. Therefore, at 273.15 K a 1 mm change in d yields an error in T_s of about 5.5 K. Thus, in practice sonic anemometers must be handled very carefully and calibrated or compared to a reference sensor frequently. Such comparisons were performed in a laboratory setting before these (and previous) experiments indicating that biases of CSAT3 temperature measurements rarely exceed 2°C; in addition, since the sonic path length is unlikely to be modified during a single

deployment, these biases tend to be constant over the whole deployment (low drift) and could therefore be corrected.

[13] In the experiments, CSAT3s were used which were newly calibrated by the manufacturer before every deployment. In addition, we checked for a potential bias and drift and applied temperature corrections to individual instruments whenever needed using the following approach. It was assumed that in the absence of shortwave radiation, i.e., at nighttime, a shielded thermistor is much less affected by radiative errors. To determine the offset of the sonic anemometer temperature, the difference between the mean nighttime (shortwave radiation <5 W m^{-2}) sonic anemometer temperature and the corresponding mean thermistor temperature was computed. This difference was used to correct the sonic anemometer temperature such that the nighttime temperatures best matched the corresponding thermistor temperatures. The drift was calculated from a linear regression of the temperature differences of the two sensors (versus time) with the slope of the fitted line being the drift. Actually, this method only provides the relative drift of two sensors; nevertheless because there was no alternative, here the drift was completely attributed to the sonic anemometer. Table 1 summarizes offset and drift for the three deployments and selected sensor pairs. Generally, the listed sensor drift is relatively small compared to the scatter in the data and the drift of the sonic temperature differs when it is computed using the Pt100 or the thermocouple as a reference; therefore, no drift correction was applied. After applying the moisture conversion and offset corrections, the CSAT3 temperature was taken as a reference being unaffected by radiation.

[14] Note that the analysis presented later in the paper will demonstrate that the differences between the various temperature measurements are very well correlated with radiation and wind speed; this excludes sonic biases or errors as a possible sources for these differences since sonic biases are not related to these effects.

4. Results and Discussion

[15] Previous studies showed that a combination of intense shortwave radiation and low-wind conditions leads to large errors in air temperature measurements. However, differences between temperature measurements of different sensors (particularly during the night) are not only the result of radiative forcing but can have several other causes. In addition to systematic and random errors, scatter in the data from the different sensors can result from different problematic conditions such as rime formation and snow/ice accretion on the sensor shield or the sensor itself. Such conditions do not only modify the radiation effects on the sensor but can also have other disturbing effects such as thermal insulation, prevention of ventilation, obstructing the transducer axes, changing the sensor albedo etc., and snowfall and blowing snow can disturb the sonic anemometer temperature measurements. Changes in local humidity due to sensor riming or drifting snow can lead to local latent heat fluxes and local temperature effects. Such events were frequently observed during the GPM observational periods leading to larger scatter in the data than in the TABLES data set.

[16] Figure 1 shows an example of how large measurement errors can be during unfavorable measurement conditions (downward shortwave radiation 800 W m^{-2}, wind speed <1 m s^{-1}) over a snow-covered area. The period shows 48 h (12–14 March 2007) of persistent clear sky conditions (Figure 1a). During the first day when daytime mean wind speed (Figure 1b) was about 7 m s^{-1}, observed differences between the shielded thermistor and the sonic anemometer temperature were on the order of 2°C, while on the next day when the average daytime wind speed was only around 1 m s^{-1}, differences reached almost 10°C (Figure 1c); one can notice that these differences are much larger than the offset corrections and drifts presented in Table 1. At night, in the absence of shortwave radiation, the measurements of the two sensors were almost identical. This example shows that even "efficient" natural ventilation of the sensor housing cannot entirely eliminate the temperature difference with respect to the reference sensor, and that only a reduction of the error from almost 10°C to about 2°C can be achieved, with a considerable residual error remaining. For the analysis below, the following classification was used: Periods when shortwave radiation was larger than 5 W m^{-2} are referred to as daytime or daylight hours, all other periods as are referred to as nighttime.

4.1. Alpine Snow-Covered Surface

[17] To identify more general patterns, we consider the distribution of temperature differences (Pt100 and CSAT3) over the day and their dependency on quantities influencing the errors using the GPM data sets. To cover a maximum of possible cases we use data of the entire measuring periods in 2007 and 2008. Figures 2a and 2d show the temperature error as a function of the time of day with the corresponding spread of the observations for each 30 min bin. Clearly, there is a strong dependence on shortwave radiation, and the spread originates from variable wind speed conditions at a given solar radiation. The higher the wind speed the smaller the temperature difference for the same shortwave radiation. Figures 2b and 2e present the frequency distribution of the errors in 0.5°C bins distinguishing daytime and nighttime hours. The majority of nighttime temperature differences appear within ±1°C. Other temperature differences within these bounds are measurements when either shortwave radiation was low or wind speed was high enough to sufficiently ventilate the sensor housing. The distributions (sum of daytime and nighttime data) are skewed with a heavy tail for positive differences up to 10°C (Figures 2b and 2e). A plot of the shielded thermistor temperature versus the sonic anemometer temperature (Figures 2c and 2f) reveals that temperature differences are generally largest during relatively warm periods. In 2008, an additionally installed thermocouple with its junction next to the CSAT3 transducer heads provided another independent measurement. The thermocouple showed smaller radiative errors with respect to the sonic anemometer temperature than the shielded thermistor (Figure 2f). Under low-wind conditions a very small sensor with little thermal inertia and a reflective surface may be less affected by solar radiation and thus be more accurate than a larger sensor in a radiation shield [*Richardson et al.*, 1999].

[18] In a next step, we look at the dependence of the temperature difference on incoming and reflected shortwave radiation, and wind speed (Figure 3). In the absence of shortwave radiation, errors are mainly within ±1°C with a few values within ±2°C. During daylight hours, both the

Table 1. Offset and Drift of Sonic Anemometer Temperature Using a Shielded Thermistor or a Thermocouple in the Absence of Shortwave Radiation as a Reference Temperature Sensor

Experiment	Reference	Offset (deg C)	Drift (deg C d^{-2})	Cumulative Drift	Period
GPM 07	Pt100	0.3535	4.13E-03	0.2604	5 Feb to 10 Apr 2007
GPM 08	Pt100	−0.4589	−3.81E-03	−0.1259	7 Feb to 11 Mar 2008
GPM 08	thermocouple	−0.1569	1.15E-02	−0.3792	7 Feb to 11 Mar 2008
TABLES	Pt100	−0.1491	2.50E-05	5.76E-04	13 Aug to 5 Sep 2008
TABLES	thermocouple	−0.0620	2.52E-05	5.79E-04	13 Aug to 5 Sep 2008

error and the spread in the error increase linearly with increasing shortwave radiation. The error's dependence on the wind speed, in contrast, shows a highly nonlinear behavior with the temperature difference drastically increasing when wind speed approaches zero. The fact that radiative errors persist even at moderate wind speed and "sufficient" ventilation of the sensor housing suggests that shielded and mechanically aspirated sensors, often being used as reference instruments for sensor (shield) intercomparisons, may also be subject to significant radiation errors when shortwave radiation, in particular reflected shortwave radiation, is large.

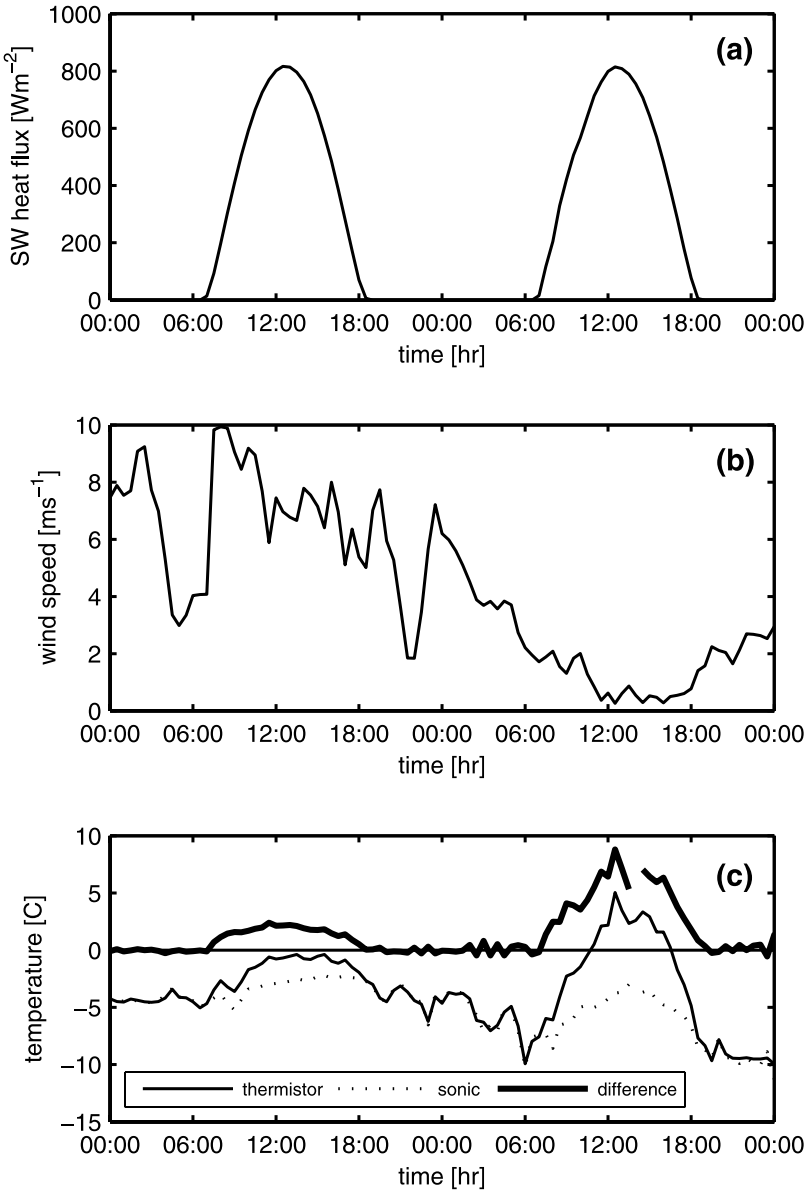

Figure 1. (a) Downwelling shortwave radiation, (b) wind speed, and (c) air temperature from a shielded thermistor and a sonic anemometer at Plaine Morte glacier, 12–14 March 2007.

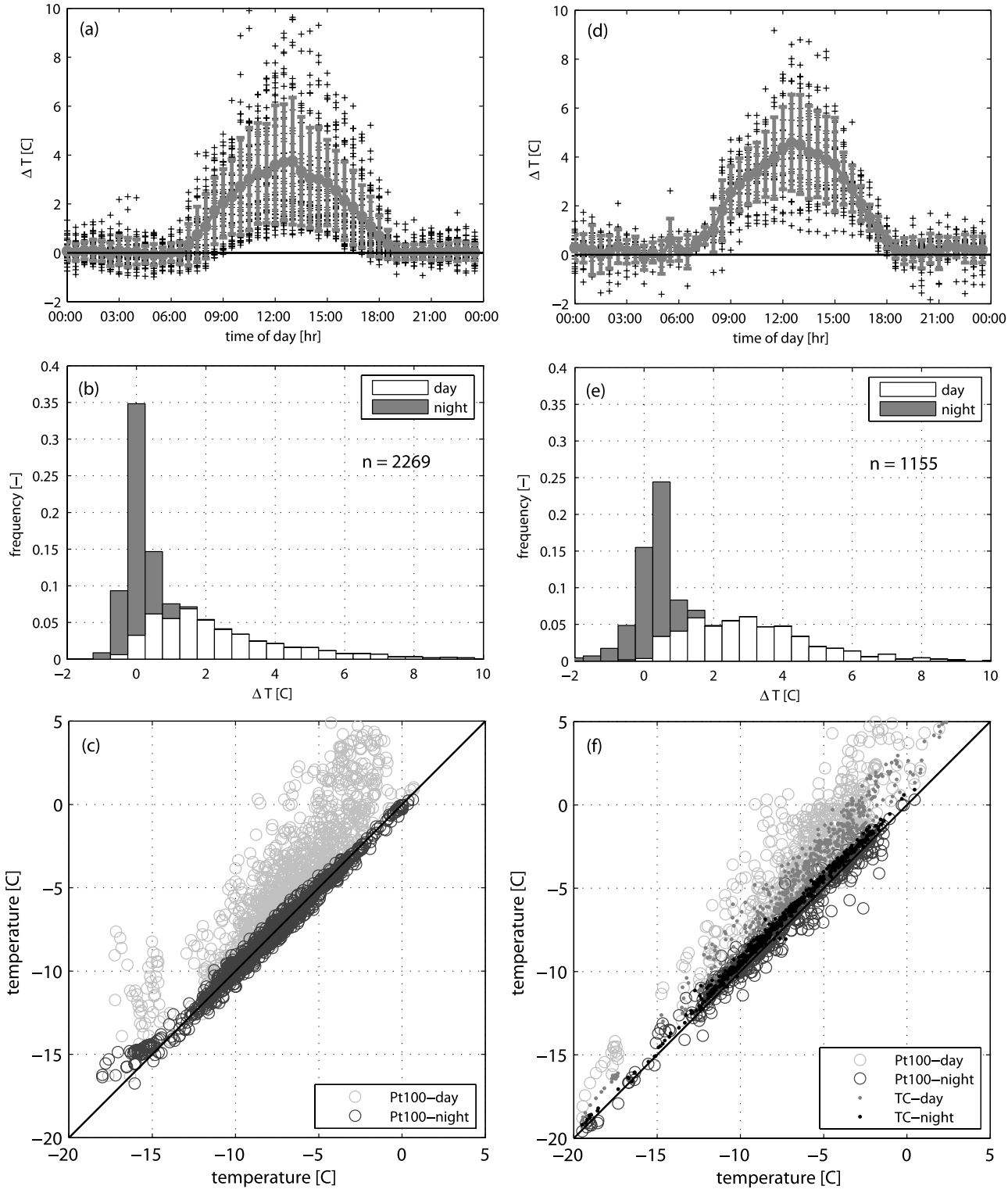

Figure 2. (a) Differences between air temperatures measured with a thermistor in a shortwave radiation shield and with a three-dimensional sonic anemometer as a function of the time of day; bars give a measure (standard deviation) of the spread in each 30 min bin. (b) Frequency distribution of temperature differences shown separately for daytime and nighttime (stacked bars). (c) Shielded thermistor temperature versus sonic anemometer temperature shown separately for daytime and nighttime. Period: 5 February through 10 April 2007. (d–f) Same as Figures 2a–2c but for the period 8 February through 11 March 2008; Figure 2f also includes a thermocouple temperature.

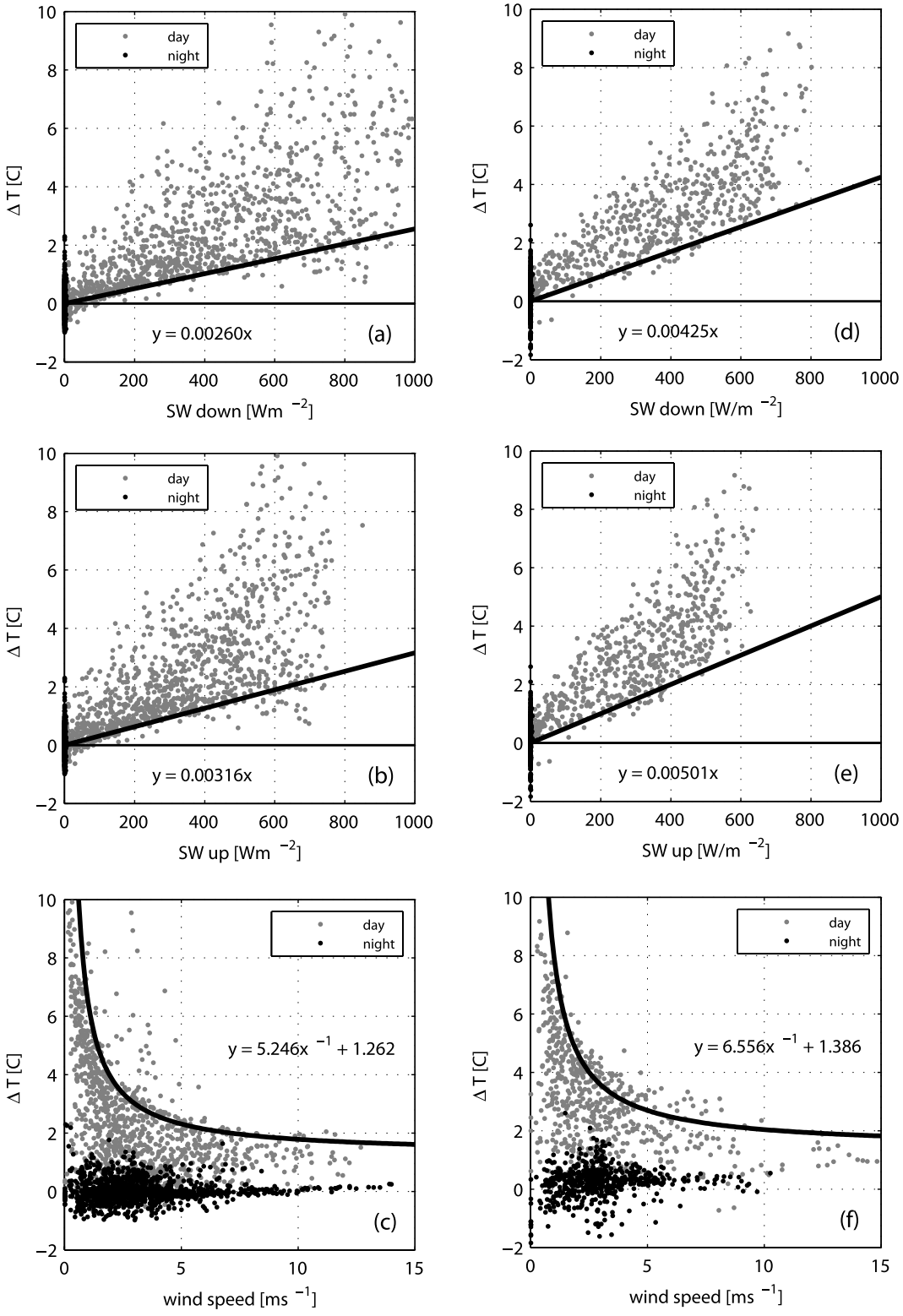

Figure 3. Differences between air temperature measurements from a shielded thermistor and a sonic anemometer versus (a) incoming shortwave radiation, (b) reflected shortwave radiation, and (c) wind speed measured at the Plaine Morte glacier from 5 February through 10 April 2007. Each data point represents a 30 min average. (d–f) same as Figures 3a–3c but for the period 8 February through 11 March 2008. The black curves are envelope lines calculated as discussed in section 4.2.

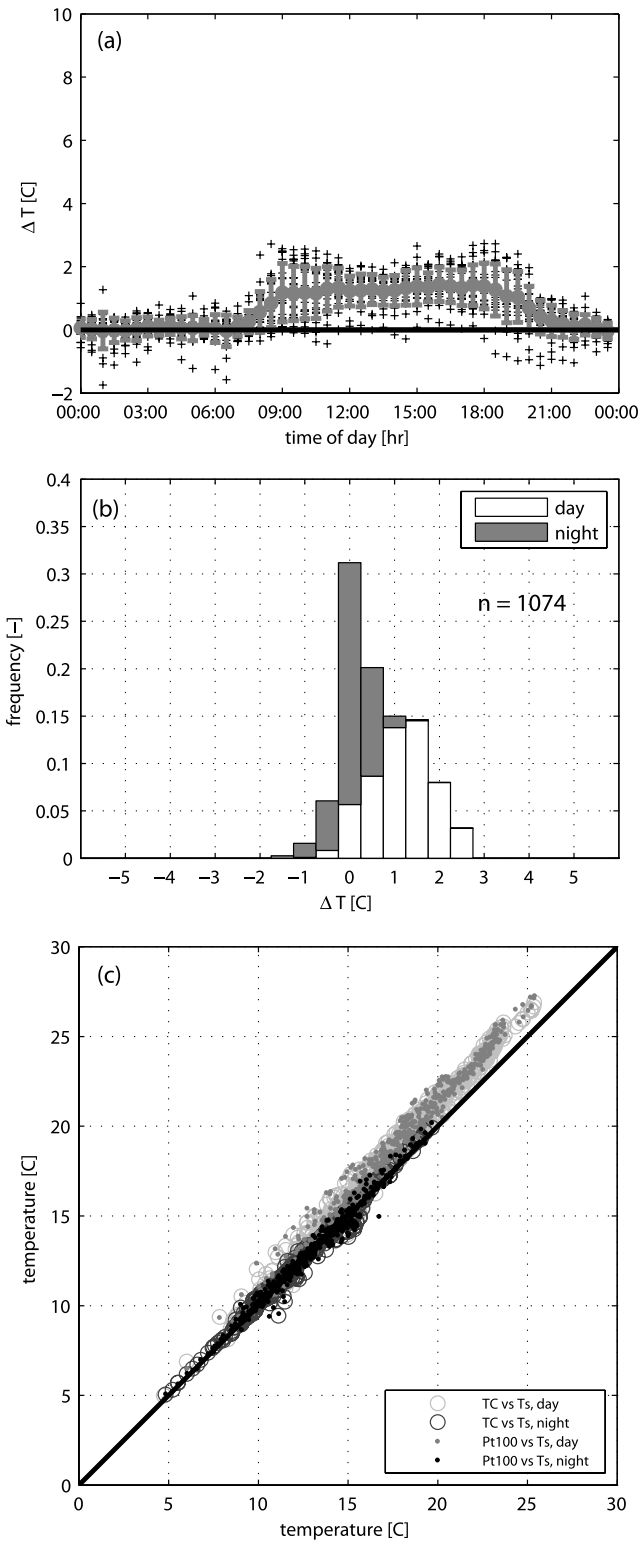

Figure 4. (a) Differences between air temperatures measured with a thermistor in a shortwave radiation shield and with a three-dimensional sonic anemometer as a function of the time of day; bars give a measure (standard deviation) of the spread in each 30 min bin. (b) Frequency distribution of temperature differences shown separately for daytime and nighttime (stacked bars). (c) Shielded thermistor and thermocouple temperature versus the sonic temperature. Period: 13 August through 5 September 2008.

4.2. Low-Land Vegetated Surface

[19] For comparison, we now investigate a different data set, namely atmospheric measurements from the TABLES experiment (see section 2). In contrast to the air temperature measurements over a snow-covered glacier, the TABLES data were collected during summer (August–September 2008) over a flat, homogeneous clover field.

[20] Looking at the magnitude and the distribution of radiation errors as a function of time of day (Figure 4a) it can be seen that (1) temperature differences between shielded thermistor and sonic anemometer are much smaller than those measured over snow and (2) the distribution is almost bimodal with peaks in the morning and late afternoon. While the former finding is a direct consequence of the surface type (discussed later), the latter can be attributed to the specific humidity conditions observed at that site. During most of the day, particularly in the early morning and late afternoon, and during the night when wind speed was usually less than 1 m s^{-1}, the air was saturated, and fog layers were present. Only during a few hours around noon relative humidity dropped to about 60%; during this period wind speed increased to above 2 m s^{-1} (no figures shown). At night, almost all of the temperature errors were within ±1°C, while during the day, errors did not exceed 3°C (Figure 4b). From Figure 4c it can be seen that for the TABLES site, in contrast to the GPM location, the radiative error of the thermistor in the multiplate shield is on the same order as that of the thermocouple sensor.

[21] Figure 5 displays the radiative errors for the TABLES site as a function of incoming and reflected shortwave radiation, and wind speed. Surprisingly, comparable amounts of shortwave radiation at both sites for generally lower wind speed at TABLES led to overall significantly smaller radiation errors at TABLES than at GPM (Figure 5; see also Figure 3 for comparison). This indicates that less radiative energy reached the shielded sensor at TABLES despite the less efficient ventilation due to lower wind speed. The main reason for this is no doubt the relatively low albedo of the clover field at TABLES (0.25 on average compared to a mean of about 0.83 for the 2007 and 2008 GPM snow cover). Indeed, it has been observed before, that reflected and diffuse components rather than direct shortwave radiation easily enter common radiation shields, leading to enhanced sensor warming [*Arck and Scherer*, 2001; *Nakamura and Mahrt*, 2005]. From Figures 5c and 3c, it can be seen that even for moderate wind speeds at a given shortwave radiation, residual errors do persist. The lower envelope lines in Figures 3a, 3b, 3d, 3e, 5a, and 5b give a measure of the minimal radiative error for a given shortwave radiation. Points close to the lower envelope of the data generally represent situations of high wind speed and most efficient sensor ventilation, while points close to an upper envelope line (not shown in figures) indicate low wind or radiation only events.

[22] The envelope lines were calculated using linear quantile regression [*Koenker*, 2005] through the origin with 10% of the points allowed below the envelope line. To avoid a negative impact of the scatter in the GPM07 temperature differences at low radiation on the envelope line (a significant fraction of data points close to $x = 0$ lies below the envelope line influencing the slope), data for

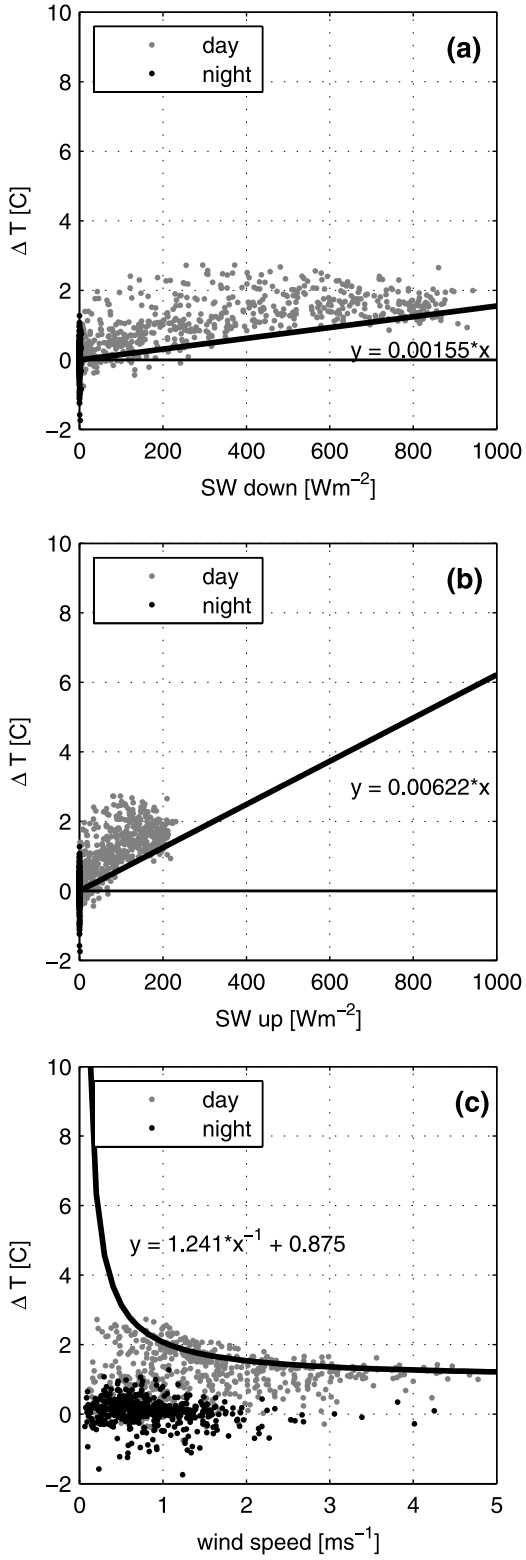

Figure 5. Differences between air temperature measurements from a shielded thermistor and a sonic anemometer versus (a) incoming shortwave radiation, (b) reflected shortwave radiation, and (c) wind speed, measured during TABLES from 13 August through 5 September 2008. Each data point represents a 30 min average. The black curves are envelope lines calculated as discussed in section 4.2.

incoming shortwave radiation less than 50 W m^{-2} were excluded from the calculation. The lower the albedo, the steeper the slope of the envelope line for the reflected shortwave radiation since the radiative error (same spread when plotted versus different quantities) is distributed over a smaller range of radiative heat fluxes. Therefore, the radiative error always grows faster with increasing reflected shortwave radiation than with the incoming radiation. This is in line with the finding that multiplate radiation shields are more sensitive to upwelling shortwave radiation than to the incident shortwave radiation [*Nakamura and Mahrt*, 2005]. Thus the radiation error is a strong function of the surface albedo which was also observed by *Lundquist and Huggett* [2008].

[23] Daily mean albedo data from all three experiments are presented in Figure 6. Over snow surfaces, the albedo ranged from 0.7 to 0.98, while over vegetated surface the variation was much smaller (0.24–0.27). The relatively large range of albedo variation over snow is mainly due to changes in the snow characteristics (e.g., fresh snow, consolidated snow, surface hoar); however, there is also an effect of rime and ice crusts forming on the glass dome of the radiometers which could not be unambiguously discriminated. Since at the given altitude (2770 m asl) melt events are rare at the time of the deployments (February to early April), the albedo never dropped below 0.7, that is into the range of melting snow (around 0.5). Daily mean albedo over the clover field in the TABLES experiment showed very little variation as a result of (1) only minor changes in the optical properties of the clover field during the observation period and (2) the absence of the problem of rime and ice formation on the instruments.

[24] From geometric considerations in Figures 3a, 3b, 3d, 3e, 5a, and 5b it follows that the slope ratio of the lower envelope lines for downward and reflected solar radiation must be equal to the albedo which is confirmed by the present results: a slope ratio of 0.82 for GPM07 and 0.85 for GPM08 as compared to the calculated mean albedo of 0.83 in both Plaine Morte winter seasons (Figure 6), and a slope ratio of 0.24 for TABLES as compared to the calculated mean of 0.25 (Figure 6).

[25] The lower envelope lines from GPM07 and GPM08 exhibit different slopes despite having the same surface type during both experiments. An obvious explanation is that the mean (median) daytime wind speed during GPM07, 3.26 m s^{-1} (2.64 m s^{-1}), was generally higher when compared to GPM08, 2.67 m s^{-1} (2.28 m s^{-1}), which can also qualitatively be seen from Figures 3c and 3f. An upper envelope line can be found analogously for the relation of the radiative error and the wind speed (Figures 3c, 3f, and 5c). However, since this relation is nonlinear, a power law of the form $y = ax^{-b} + c$ with an asymptotic behavior and an offset c for increasing values of x is better suited, as beyond a certain point the radiation error will no longer decrease for increasing wind speed due to a constrained maximum ventilation efficiency. Similarly, the radiation error is likely to approach a maximum level for increasing radiation, and it would be possible to fit nonlinear envelope curves. However, the maximum values of wind speed and shortwave radiation measured during the experiments are close to their natural upper limit at each location and therefore more

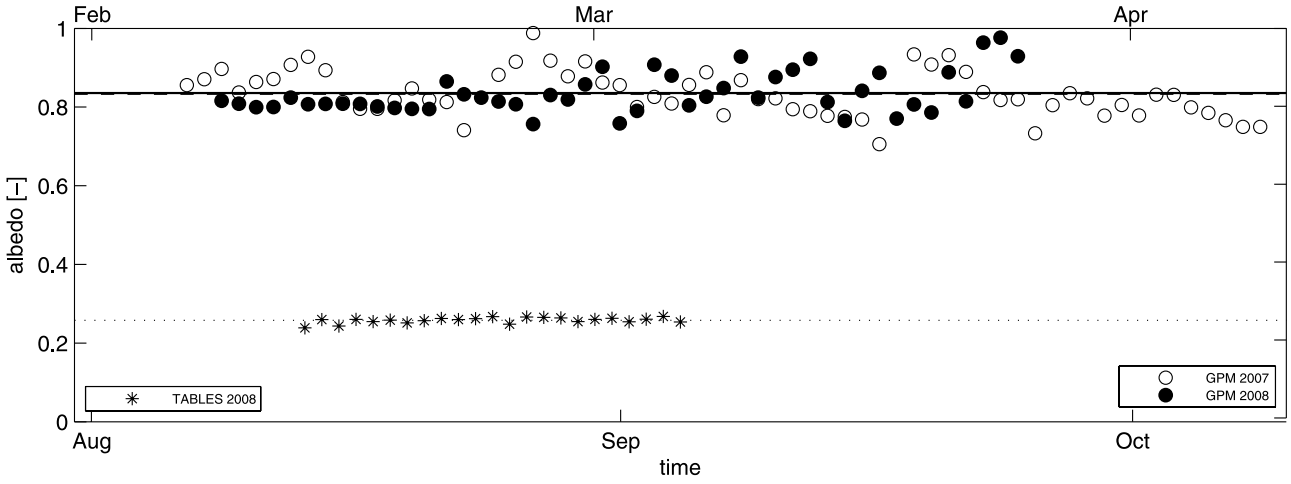

Figure 6. Daytime mean albedo during the GPM07, GPM08, and TABLES experiments. Horizontal lines denote mean albedo value during the corresponding observation period (GPM07, dashed line; GPM08, solid line; TABLES, dotted line). GPM experiments are plotted on the top time axis.

elaborate descriptions would not lead to very different envelope curves.

4.3. Ventilated Sensors

[26] The dominant effect of the surface albedo on instrument temperature can be demonstrated by taking advantage of another independent set of installed sensors, namely the four radiometers. Each of the two pyranometers (sky and surface facing) and two pyrgeometers (sky and surface facing) has a built-in thermistor to determine the thermopile temperature; each radiometer is actively ventilated by a fan positioned directly below the sensor in an attempt to keep it at the actual ambient temperature. Therefore, the built-in thermistors can be viewed as surrogates for mechanically ventilated air temperature sensors. The upper and lower pairs of sensors are absolutely symmetric in terms of their geometry and materials. Despite the fact that the built-in thermistors are not measuring air temperature (during the day they measure temperature being a bit higher than the air temperature due to shortwave absorption of the sensor disc), they still provide some useful information on the thermal state of the instrument. As a result of the high snow albedo at Plaine Morte, the surface facing sensors receive on the order of 85% of the incoming shortwave radiation, an amount of energy comparable to that received by the upward looking sensors. That is, over snow all four sensors are exposed to similarly large amounts of radiation during daylight hours which underlines the importance of surface-reflected shortwave radiation.

[27] To demonstrate the influence of surface-reflected shortwave radiation, we compare the two sky facing sensors to the surface facing sensors by first computing the mean of two sensors of the same orientation and then calculating the mean difference between upper and lower sensors. During the day, downward looking sensors are mostly shaded by the upper sensors and thus mainly exposed to reflected shortwave radiation. For both glacier deployments, the mean differences between upper and lower sensors for daytime are smaller than 0.1°C (Table 2). At the TABLES site, however, the mean daytime difference is 0.62°C, being significantly larger than in the two glacier experiments. During the night, the upper sensors are consistently colder than the lower sensors in all three experiments with the TABLES site showing the largest difference and the smallest spread when compared to the data from the glacier (Table 2). The daily averages are less meaningful, since they include the compensating day-night effects. Figure 7 shows the relation of the upper versus the lower sensors for all three experiments. The measurements over snow (Figures 7a and 7b) show little scatter, which means small differences between sky and surface facing sensors for all times of the day. Differences are larger at the TABLES site (Figure 7c), even changing sign from daytime to nighttime (see also Table 2).

[28] In summary, the radiometer thermistors measure temperatures higher than the air temperature during the day, and there is an influence of radiative processes on the sensor temperature despite the mechanical ventilation and symmetric configuration. During the day, shortwave radiation leads to heating of the sensor enclosures, which transfer part of this energy radiatively or conductively to the sensor. Conversely, it appears that during the night there is a small error of the opposite sign due to differential radiative cooling (radiation received from surface and atmosphere minus radiation emitted by instrument equals heat loss) of the instruments. This is a direct consequence of the longwave radiation balance which is usually strongly negative both for the snow surface on the glacier and for the clover field [*Hoch et al.*, 2007]. That is, the downward looking sensors receive more longwave radiation than the sky facing sensors as a result of the surface-atmosphere temperature difference and the difference in emissivity between surface (snow: ~0.99) and a clear sky atmosphere (~0.70).

4.4. Scaling Model

[29] To precisely correct for radiative errors, the effective ventilation and amount of radiation inside the shield must be known; however, these are difficult to measure. Easily applicable correction methods should be based on routinely measured quantities, ideally those with the greatest impact

Table 2. Mean Temperature Differences Between the Average of Sky Facing and the Average of Surface Facing Radiometers for Pyranometer and Pyrgeometer Pairs[a]

	GPM07		GPM08		TABLES	
	Avg	SD	Avg	SD	Avg	SD
All	−0.23	0.41	−0.15	0.30	0.16	0.85
Day	−0.08	0.46	−0.02	0.35	0.62	0.90
Night	−0.35	0.30	−0.25	0.19	−0.42	0.18

[a]Avg, average; SD, standard deviation.

on the radiative error. Such variables are shortwave radiation and wind speed. One framework using these quantities is the similarity regression model proposed by *Nakamura and Mahrt* [2005], which scales radiation with wind speed, measured air temperature and air properties to a nondimensional number, as follows:

$$C = \frac{SW}{\rho c_p u T}, \tag{5}$$

where SW is the incoming solar radiation, ρ and c_p are the density and specific heat at constant pressure of air, respectively, u is the wind speed, and T the measured air temperature. A correction function of the given type will still show some scatter, since solar radiation and wind speed are independent and uncorrelated variables. However, it provides general information on how radiative errors are related to actual meteorological conditions. Also the correction model proposed by *Arck and Scherer* [2001] is based on observations of wind speed and solar radiation in addition to the measured air temperature. Here we apply the regression model of *Nakamura and Mahrt* [2005] using the data sets obtained during the three field campaigns at the high Alpine and the farmland sites (Figure 8a). A comparison shows that the range of observed radiative errors and values of the nondimensional radiation forcing is much larger for the data from the glacier site than in the data from the grass land site (up to 10°C compared to about 2°C). The GPM data sets demonstrate that the value of the nondimensional radiation forcing grows faster for increasing radiative error. This nonlinear behavior is not obvious in the grassland data of *Nakamura and Mahrt* [2005].

[30] The nondimensional scaling of the TABLES data results in a very different pattern compared to the GPM data with the slope of a regression curve always lower than the glacier data. This indicates that the scaling does not completely account for all or most of the relevant variables. For an optimal scaling, the resulting nondimensional radiation forcing functions for each data set should collapse to a single line. This seems to be already the case for the two glacier data sets. While solar radiation and wind speed are comparable in magnitude for the GPM and the TABLES data, there is a major difference in the mean albedo (0.83 for GPM and 0.25 for TABLES). Thus, inclusion of the albedo α in the scaling as a factor for the incident solar radiation (which is equivalent to directly using the reflected shortwave radiation as measured) yields

$$C = \frac{\alpha SW\downarrow}{\rho c_p u T} = \frac{SW\uparrow}{\rho c_p u T}. \tag{6}$$

This way, data from different locations with very different surface properties are more likely to collapse such that they can be approximated with a single regression curve. Indeed, Figure 8b confirms that reflected shortwave radiation is

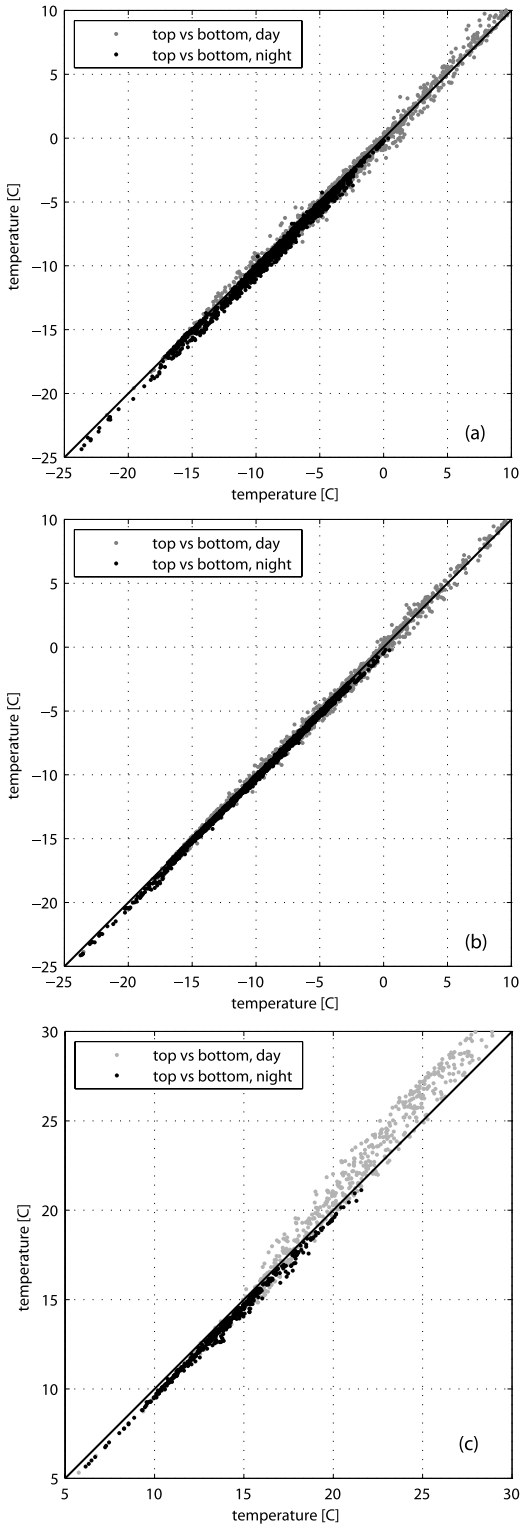

Figure 7. Mean of the sky facing pyranometer-pyrgeometer pair thermistor temperature versus the mean of the surface facing pyranometer-pyrgeometer pair thermistor temperature for (a) GPM07, (b) GPM08, and (c) TABLES experiments.

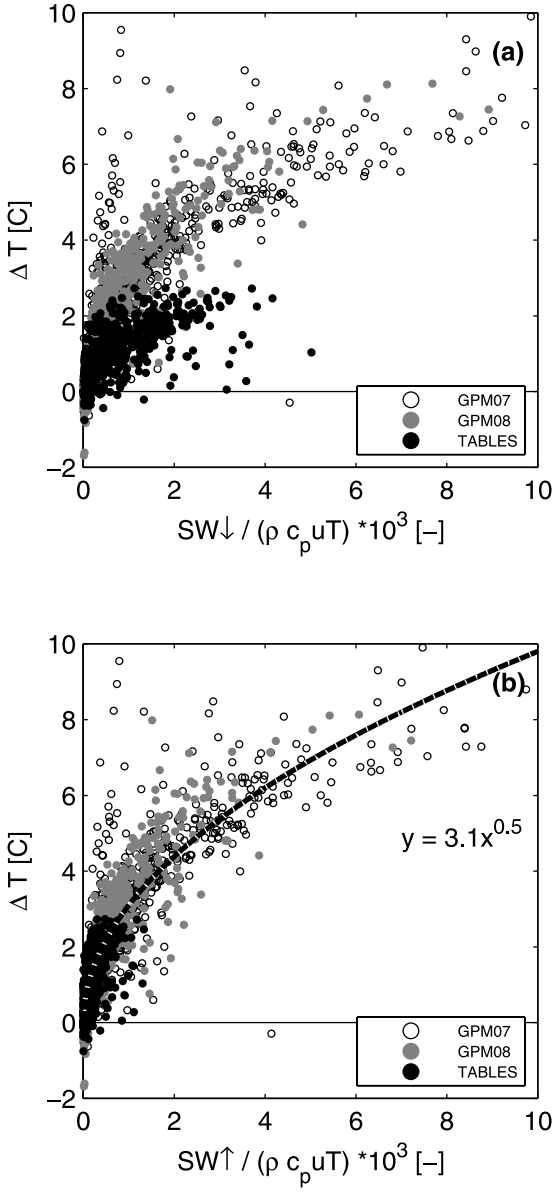

Figure 8. Radiative error versus the nondimensional scaling term for Plaine Morte 2007, 2008, and TABLES deployments. (a) Measured incident shortwave radiation (surface albedo not considered) and (b) measured reflected solar radiation (surface albedo taken into account). For better display, the scaling term is multiplied by a factor 10^3 (the temperature in this term is expressed in Kelvin). The dashed line in Figure 8b is a best fit power law of the form $y = ax^b$ (negative values excluded).

more relevant than incoming solar radiation, and supports the validity of the new scaling. This result is in agreement with earlier studies which mention the dominant role of the reflected shortwave radiation on the radiative errors in naturally ventilated air temperature sensor shields [*Arck and Scherer*, 2001; *Georges and Kaser*, 2002; *Nakamura and Mahrt*, 2005]. The latter study discovered through measurements over three different surface types (grass field, black and white tarp) a positive correlation of the surface albedo and the shortwave radiation entering the shield. It also found that the reflected shortwave radiation is the source of a large fraction of the solar radiation reaching inside the shield. In other words, the radiative error is a strong function of the surface albedo. The new scaling no longer requires the calculation of different coefficients of the regression polynomial for different surface types as necessary in the previous scaling [*Nakamura and Mahrt*, 2005, equation (5)]. While this model is universal in the sense that it applies for all surfaces, the fit should be performed for each sensor/shield combination separately.

[31] Reflected shortwave radiation and wind speed are routinely measured on many automatic weather stations and therefore available for the new scaling and air temperature correction. For instance, the IMIS system, a network of about 200 stations in the Swiss Alps at altitudes from 2000 to 3500 m, successfully measures reflected shortwave radiation for several practical reasons (sensor is less likely to be snow covered and rimed) as the only radiative flux term for high Alpine sites [*Lehning et al.*, 2002]. As a consequence, the corrected air temperatures will improve snow cover modeling as done operationally on the IMIS network.

5. Conclusions

[32] The combination of incident solar radiation and low-wind conditions leads to significant errors in air temperature measurements when using a sensor installed in a naturally ventilated radiation shield. These radiative errors tend to be particularly large over snow-covered surfaces (up to 10°C). To quantify radiative errors of different sensor/shield systems, mechanically ventilated instruments are usually used as a reference sensor. Since none of these sensors measures temperature without being influenced by sensible, conductive and radiative heat transfer, it is not clear if and by how much reference sensors are biased. We propose a sonic anemometer as a possible temperature reference, as this instrument measures the temperature of an air volume without being affected by radiation, heat conduction, and sensible heat. However, care has to be taken to account for possible offset or drift of the instrument due to mechanical shock and mishandling that could alter the exact sonic path length. The offset of the sonic anemometer temperature was corrected using nighttime temperature data (unaffected by solar radiation) of a reference sensor.

[33] In this study, radiative errors from three different measuring campaigns at two very different places, a snow-covered glacier and a farmland clover field, were investigated, identifying their temporal distribution as well as the main physical processes responsible for the errors. Radiative errors are strong functions of solar radiation and wind speed. Radiative errors from a thermistor installed in a multiplate radiation shield are drastically reduced under high wind speed conditions for a given (large) solar radiation but do not completely disappear when compared to the radiation independent reference temperature from the sonic anemometer. Temperature measurements from an unshielded thermocouple over a snow surface are less affected by solar radiation than a thermistor in a classical multiplate naturally ventilated radiation shield due to its small size, reflective properties and fast response time to wind cooling.

[34] Radiative errors grow faster with increasing reflected shortwave than with incident solar radiation since the same

errors are distributed over a smaller range of radiative heat flux values. The ratio of lower envelope curves of the radiation error as a function of incident and reflected solar radiation is equal to the mean albedo at the measurement site. This property appears in the data from three independent campaigns at two different sites. Radiative errors are strongly surface type–dependent, that is, they are a strong function of the surface albedo.

[35] Although not directly measuring air temperature, an albedo effect is also seen in temperatures from radiometer built-in thermistors despite mechanical ventilation. Over snow, the daytime mean temperature of the two sky facing sensors closely agrees with the daytime mean of the two surface facing instruments, while over a clover field, the upper sensor pair was warmer than the lower pair during the day. This is a direct consequence of the surface albedo, where the amount of energy reaching the surface facing sensors over snow is not much smaller than the exposure to incident radiation for the upper pair.

[36] Several methods have been proposed to correct for the radiative errors, one of them proposing a similarity regression model which scales the radiation with the volumetric internal energy of the air, and the wind speed [*Nakamura and Mahrt*, 2005]. Applying the regression model to data from sites with different surface types results in multiple expressions of a similarity model. Only when accounting for the surface albedo, that is, when the similarity model is written using the reflected instead of the incident shortwave radiation, a collapse of the regression lines for the different surfaces into one universal line is obtained. For large radiative errors, when higher-order terms become relevant, it is appropriate to use a nonlinear regression model. The present study clearly identifies the importance of the surface albedo and the predominant effect of reflected solar radiation on radiative errors, in agreement with similar findings in the recent literature.

[37] **Acknowledgments.** The authors thank P. Schibli, Crans-Montana ski resort, and his team for the logistical support to carry out the measurements on the glacier. We also thank the town of Lenk for permission to conduct measurements on Plaine Morte glacier and S. Schmitter for permission to measure at the Seedorf site. We acknowledge substantial help on the glacier from M. Calaf and J. Overney, and we appreciate the help of K. Schroff, who gave useful technical advice for the design of the meteorological station. We thank W. Brutsaert for competent input to improve the manuscript, and also J. Lundquist and an anonymous reviewer for their valuable comments which enhanced the quality of this paper. This work was funded by SNF grant 200021-109566/1.

References

Anderson, S. P., and M. F. Baumgartner (1998), Radiative heating errors in naturally ventilated air temperature measurements made from buoys, *J. Atmos. Oceanic Technol.*, *15*, 157–173, doi:10.1175/1520-0426(1998)015<0157:RHEINV>2.0.CO;2.

Arck, M., and D. Scherer (2001), A physically based method for correcting temperature data measured by naturally ventilated sensors over snow, *J. Glaciol.*, *47*(159), 665–670, doi:10.3189/172756501781831774.

Braithwaite, R., and Y. Zhang (2000), Sensitivity of mass balance of five Swiss glaciers to temperature changes assessed by tuning a degree-day model, *J. Glaciol.*, *46*(152), 7–14, doi:10.3189/172756500781833511.

Brutsaert, W., and M. B. Parlange (1992), The unstable surface layer above forest: Regional evaporation and heat flux, *Water Resour. Res.*, *28*, 3129–3134, doi:10.1029/92WR01860.

Erell, E., V. Leal, and E. Maldonado (2005), Measurement of air temperature in the presence of a large radiant flux: An assessment of passively ventilated thermometer screens, *Boundary Layer Meteorol.*, *114*, 205–231, doi:10.1007/s10546-004-8946-8.

Fleagle, R. G., and J. A. Businger (1980), *An Introduction to Atmospheric Physics*, 432 pp., Academic, San Diego, Calif.

Fuchs, M., and C. B. Tanner (1965), Radiation shields for air temperature thermometers, *J. Appl. Meteorol.*, *4*, 544–547, doi:10.1175/1520-0450(1965)004<0544:RSFATT>2.0.CO;2.

Georges, C., and G. Kaser (2002), Ventilated and unventilated air temperature measurements for glacier-climate studies on a tropical high mountain site, *J. Geophys. Res.*, *107*(D24), 4775, doi:10.1029/2002JD002503.

Gil, G. C. (1983), Comparison testing of selected naturally ventilated solar radiation shields, technical report, Natl. Data Buoy Cent., NOAA, Stennis Space Center, Miss.

Hardy, D. R., M. Vuille, C. Braun, F. Keimig, and R. S. Bradley (1998), Annual and daily meteorological cycles at high altitude on a tropical mountain, *Bull. Am. Meteorol. Soc.*, *79*, 1899–1913, doi:10.1175/1520-0477(1998)079<1899:AADMCA>2.0.CO;2.

Hoch, S. W., P. Calanca, R. Philipona, and A. Ohmura (2007), Year-round observation of longwave radiative flux divergence in Greenland, *J. Appl. Meteorol. Climatol.*, *46*, 1469–1479, doi:10.1175/JAM2542.1.

Hock, R. (1994), Comparison of ventilated and unventilated temperature measurements, *Tarfala Res. Stn. Annu. Rep. 1992–93*, Dep. of Phys. Geogr., Stockholm Univ., Stockholm.

Hock, R. (1999), A distributed temperature-index ice- and snowmelt model including potential direct solar radiation, *J. Glaciol.*, *149*, 101–111.

Hubbard, K. G., X. Lin, and E. A. Walter-Shea (2001), The effectiveness of ASOS, MMTS, Gill and CRS air temperature radiation shields, *J. Atmos. Oceanic Technol.*, *18*, 851–864, doi:10.1175/1520-0426(2001)018<0851:TEOTAM>2.0.CO;2.

Kaimal, J. C., and J. E. Gaynor (1991), Another look at sonic thermometry, *Boundary Layer Meteorol.*, *56*, 401–410, doi:10.1007/BF00119215.

Katul, G. G., and M. B. Parlange (1995), Analysis of land surface heat fluxes using the orthonormal wavelet approach, *Water Resour. Res.*, *31*, 2743–2749, doi:10.1029/95WR00003.

Kent, E. C., R. Tiddy, and P. Tylor (1993), Correction of marine air temperature observations for solar radiation effects, *J. Atmos. Oceanic Technol.*, *10*, 900–906, doi:10.1175/1520-0426(1993)010<0900:COMATO>2.0.CO;2.

Koenker, R. (2005), *Quantile Regression*, 349 pp., Cambridge Univ. Press, New York.

Lehning, M., P. Bartelt, B. Brown, and C. Fierz (2002), A physical SNOWPACK model for the Swiss avalanche warning: Part III: Meteorological forcing, thin layer formation and evaluation, *Cold Reg. Sci. Technol.*, *35*, 169–184, doi:10.1016/S0165-232X(02)00072-1.

Lin, X., K. G. Hubbard, and G. E. Meyer (2001), Airflow characteristics of commonly used temperature radiation shields, *J. Atmos. Oceanic Technol.*, *18*, 329–339, doi:10.1175/1520-0426(2001)018<0329:ACOCUT>2.0.CO;2.

Lundquist, J. D., and B. Huggett (2008), Evergreen trees as inexpensive radiation shields for temperature sensors, *Water Resour. Res.*, *44*, W00D04, doi:10.1029/2008WR006979.

Mauder, M., R. L. Desjardins, Z. Gao, and R. van Haarlem (2008), Errors of naturally ventilated air temperature measurements in a spatial observation network, *J. Atmos. Oceanic Technol.*, *25*, 2145–2151, doi:10.1175/2008JTECHA1046.1.

Nakamura, R., and L. Mahrt (2005), Air temperature measurement errors in naturally ventilated radiation shields, *J. Atmos. Oceanic Technol.*, *22*, 1046–1058, doi:10.1175/JTECH1762.1.

Ohmura, A. (2001), Physical basis for the temperature-based melt-index method, *J. Appl. Meteorol.*, *40*, 753–761, doi:10.1175/1520-0450(2001)040<0753:PBFTTB>2.0.CO;2.

Payne, R. E. (1987), Air temperature shield tests, technical report, Woods Hole Oceanogr. Inst., Woods Hole, Mass.

Richardson, S. J., F. V. Brock, S. R. Semmer, and C. Jirak (1999), Minimizing errors associated with multiplate radiation shields, *J. Atmos. Oceanic Technol.*, *16*, 1862–1872, doi:10.1175/1520-0426(1999)016<1862:MEAWMR>2.0.CO;2.

M.-O. Boldi, C. W. Higgins, H. Huwald, and M. B. Parlange, School of Architecture, Civil and Environmental Engineering, Ecole Polytechnique Fédérale de Lausanne, Batiment GR, Station 2, CH-1015 Lausanne, Switzerland. (hendrik.huwald@epfl.ch)

E. Bou-Zeid, Department of Civil and Environmental Engineering, Princeton University, Princeton, NJ 08540, USA.

M. Lehning, WSL Institute for Snow and Avalanche Research SLF, Davos, CH-7260 Switzerland.